

# Strength Characteristics of a Heat-Resistant Metal-Matrix Composite Inconel 625–5%NiTi–TiB<sub>2</sub> Alloy Fabricated by Direct Laser Deposition under Shock-Wave Loading

Sergey Razorenov <sup>1</sup>, Gennady Garkushin <sup>1</sup> , Andrey Savinykh <sup>1</sup> , Vladimir Promakhov <sup>2,\*</sup>, Alexey Matveev <sup>2</sup> , Olga Klimova-Korsmik <sup>3</sup> and Alexander Vorozhtsov <sup>2</sup>

<sup>1</sup> Federal Research Center of Problems of Chemical Physics and Medicinal Chemistry RAS, 142432 Chernogolovka, Russia

<sup>2</sup> Faculty of Physics and Engineering, National Research Tomsk State University, 36 Lenin Avenue, 634050 Tomsk, Russia

<sup>3</sup> Department of Digital Industrial Technology, St. Petersburg Marine Technical University, Lotsmanskaya, 3, 190121 St. Petersburg, Russia

\* Correspondence: vvpromakhov@mail.ru

**Abstract:** The Hugoniot elastic limit and spall strength were measured for a heat-resistant metal-matrix composite Inconel 625–5%NiTi–TiB<sub>2</sub> alloy additive manufactured (AM) by direct laser deposition. The strength characteristics of the alloy were obtained from the analysis of the complete wave profiles recorded with a VISAR laser Doppler velocimeter during shock-wave loading of the samples. The samples were loaded using a PP50 pneumatic gun or ad hoc explosive devices along and across the material deposition direction in order to determine the strength anisotropy of the AM alloy under study. The maximum shock compression pressure was ~7 GPa, and the strain rate under tension before spalling varied in the range of 10<sup>5</sup>–10<sup>6</sup> s<sup>−1</sup>. Kinetic dependencies of elastic/plastic transition and critical fracture stresses vs. loading conditions were plotted. It was shown that the Hugoniot elastic limit of the alloy under study decreases as the shock wave travels into the sample, while the spall strength increases as the material's strain rate increases at the moment of spall fracture. A comparison of the strength characteristics of the Inconel 625–NiTi–TiB<sub>2</sub> composite alloy with the original Inconel 625 alloy has shown that an addition of 5% of powder based on NiTi–TiB<sub>2</sub> leads to a decrease in its elastic limit and critical fracture stresses upon spalling by more than 10%. The alloy under study demonstrates anisotropy of strength properties relative to the material deposition direction.

**Keywords:** additively manufactured heat-resistant alloy; metal-matrix composite Inconel 625–5%NiTi–TiB<sub>2</sub>; direct laser deposition; shock-wave loading; Hugoniot elastic limit; spall strength



**Citation:** Razorenov, S.; Garkushin, G.; Savinykh, A.; Promakhov, V.; Matveev, A.; Klimova-Korsmik, O.; Vorozhtsov, A. Strength Characteristics of a Heat-Resistant Metal-Matrix Composite Inconel 625–5%NiTi–TiB<sub>2</sub> Alloy Fabricated by Direct Laser Deposition under Shock-Wave Loading. *Metals* **2023**, *13*, 477. <https://doi.org/10.3390/met13030477>

Academic Editors: Hany Hassanin and Pavel Krakhmalev

Received: 8 December 2022

Revised: 10 January 2023

Accepted: 4 February 2023

Published: 25 February 2023



**Copyright:** © 2023 by the authors. Licensee MDPI, Basel, Switzerland. This article is an open access article distributed under the terms and conditions of the Creative Commons Attribution (CC BY) license (<https://creativecommons.org/licenses/by/4.0/>).

## 1. Introduction

Heat-resistant alloys of the Inconel brand have proven themselves as functional materials with advanced mechanical properties operating at high temperatures and loads in chemically aggressive environments [1,2]. Specifically, Inconel 625 has excellent mechanical properties and excellent resistance to pitting, crevice, erosion and intergranular corrosion as well as insensitivity to corrosion cracking and good resistance to nitric, phosphoric, sulfuric, hydrochloric and organic acids. According to a series of research papers, a combination of advantages of additive manufacturing technologies with improved mechanical properties of Inconel alloys makes it possible to cost-effectively produce products with complex geometries, such as turbines and engine injectors, complex pipeline joints, etc., operating under extreme conditions: high temperatures, high mechanical stress and pressures, etc. [3–6]. Despite the fact that Inconel 625 alloys have advanced mechanical properties over a wide range of operating temperatures, new designs and products are constantly being developed in different industries and they require still better performance [7]. One of the methods for

improving physical and mechanical properties of materials is the creation of metal-matrix composites. The structure of these composites consists of a metal/intermetallic matrix wherein ceramic inclusions are uniformly distributed [8,9]. With the inclusion of ceramic particles, composites have higher mechanical strength as compared to traditional alloys, and these particles also increase composites' durability and wear resistance at higher operating temperatures [10–13]. Metal-matrix composites are mostly made from a mixture of Inconel powders (base) and ceramic powders: TiC [14], WC [15] and CrC [16], etc. However, use of such a powder mixture is very often accompanied by agglomeration of ceramic particles in the process of composite material fabrication by direct laser deposition. Agglomeration of ceramic particles leads to the formation of a heterogeneous structure in the composite material and the emergence of depleted zones (i.e., areas without ceramic inclusions), which significantly worsens composites' mechanical properties. The authors of works [17–19] have demonstrated successful use of the NiTi–TiB<sub>2</sub> powder as a dopant (5 wt. %) to Inconel 625. The NiTi–TiB<sub>2</sub> powder was obtained by self-propagating high-temperature synthesis from a NiB–Ti powder mixture [17]. The powder particles consisted of an intermetallic NiTi matrix and TiB<sub>2</sub> ceramic inclusions distributed within it. During direct laser deposition, the matrix melt wetted ceramic particles, thus allowing them to be evenly distributed in the base Inconel 625 melt. In addition, the matrix melt hindered the agglomeration and recrystallization of TiB<sub>2</sub> particles. The authors of [17–19] found that the addition of 5 wt. % NiTi–TiB<sub>2</sub> resulted in increased hardness as well as tensile, compressive, and three-point bending strength, both at room and elevated temperatures as compared to pure Inconel 625 alloy. Despite widespread use of additive materials in many industries, data on their dynamic properties under impulse loading are scarce. The results of measurements of the strength characteristics under impact loading of high-strength steels [20,21], titanium [22–24], aluminium alloys [25], tantalum [26], and, more recently, high-temperature INCONEL alloys [27–29] with an intensity of up to 7 GPa are known. However, they do not include a well-defined response of AM metals and alloys to dynamic loading. In most cases, AM materials demonstrate strength properties that are at least as good, or, in some cases, much better than those of their counterparts produced using conventional technologies. Rarely, there is a deterioration in their strength characteristics and anisotropy of these characteristics that correlates with the texture formed due to fabrication process peculiarities.

The purpose of this work is to study the strength properties of the following composite alloy: Inconel 625 + 5 wt. % NiTi–TiB<sub>2</sub> fabricated by direct laser deposition under shock-wave loading with the intensity up to 13 GPa.

## 2. Materials and Methods

### 2.1. Fabrication of Samples by Direct Laser Deposition

Inconel 625 powders (Hoganas) and NiTi–TiB<sub>2</sub> composite powder were used to fabricate samples by direct laser deposition. The sizes of ceramic inclusions ranged between 40 and 180 µm while the average size was 90 µm. The NiTi–TiB<sub>2</sub> powder was obtained by self-propagating high-temperature synthesis from a NiB–Ti powder mixture [17]. The average particle size of titanium diboride in the intermetallic matrix was 0.5 µm, and the largest contribution to the distribution was made by particles with the size ranging from 0.1 to 0.2 µm. The Inconel 625 and NiTi–TiB<sub>2</sub> powders were mixed at the following ratio: 95 wt. % Inconel 625 + 5 wt. % NiTi–TiB<sub>2</sub>. The mixture was stirred in a ball mill for 30 min. Massive samples were obtained by direct laser deposition of the powder mixture on a substrate made of 7 mm thick RCE36 steel. An industrial robot M20iB/25 (Fanuc, Oshino-mura, Japan), LS-3 ytterbium fiber laser (IPG Photonics, Oxford, MA, USA) was used for deposition. Laser radiation was focused using an FLW D30 process (IPG Photonics, Oxford, MA, USA). A SO12 coaxial deposition nozzle (ILWT, Saint-Petersburg, Russia) was used to form the gas-powder jet and a 5.0 APS Powder insert powder feeder (Oerlikon, Freienbach, Switzerland). The process of depositing samples from 95% (Inconel 625) + 5% (NiTi–TiB<sub>2</sub>) by the AM process was carried out in argon atmosphere at a radiation power of

1200 W, and the process rate was 25 mm/s with a beam diameter of 2 mm. The workpieces obtained in this way were homogeneous, they did not contain visible discontinuities and large foreign inclusions. An image of a fabricated workpiece of a high-temperature 95% Inconel 625 + 5% NiTi–TiB<sub>2</sub> composite alloy is shown in Figure 1a. The X-ray pattern of the fabricated composite as well as its structure and a histogram of TiB<sub>2</sub> ceramic particle sizes distribution are shown in Figure 1b–d.

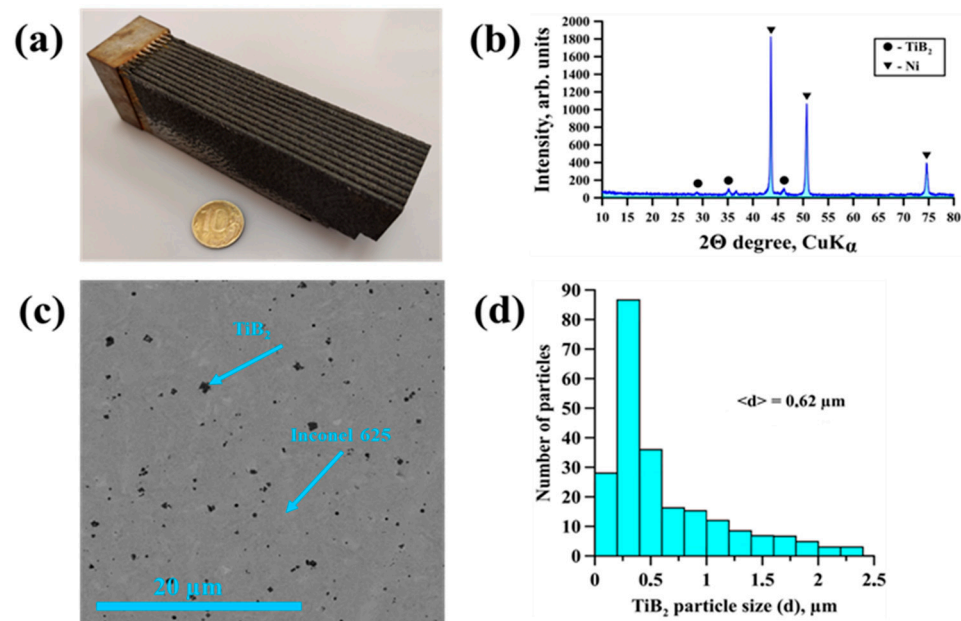


**Figure 1.** Appearance of a workpiece made of a high-temperature composite Inconel 625 + 5 wt.% NiTi–TiB<sub>2</sub> (a) alloy, X-ray and SEM images of the workpiece structure (b,c), histogram of the distribution of TiB<sub>2</sub> ceramic inclusions in the structure of the composite workpiece (d).

The density measured using hydrostatic weighing on a Mettler Toledo ME204T (Shanghai, China) high-precision analytical balance was 8.24 g/cm<sup>3</sup>. The original Inconel 625 alloy had a density of 8.44 g/cm<sup>3</sup>. The MGNIVP “Akustika” (Saint-Peterburg, Russia) device was used for measuring the velocity of propagation of acoustic waves, and the longitudinal sound speeds  $c_l$  of the samples along and across the direction of deposition were  $5.784 \pm 10$  km/s and  $5.616 \pm 10$  km/s, respectively.

The microhardness of the 95% Inconel 625 + 5% NiTi–TiB<sub>2</sub> alloy varied from 4.24 to 4.54 GPa, and the average microhardness was  $4.42 \pm 0.1$  GPa, while its distribution over the sample was determined as linear. The average microhardness of the pure Inconel 625 measured for the sake of comparison was  $2.73 \pm 0.1$  GPa. Thus, adding 5 wt.% of NiTi–TiB<sub>2</sub> composite metal matrix powder to Inconel 625 powder results in increasing of the material microhardness by 1.5 times.

## 2.2. Shock-Wave Loading of the Samples

For shock-wave experiments, plane-parallel samples with a thickness ranging from 0.2 mm to 3 mm were cut from the workpiece (Figure 1) on an ARTA 120 machine (Phryazino, Moscow reg., Russia) using the electroerosion method. This was followed by manual machining (grinding and polishing) of the surface to bring it to the reflectivity required for recording its velocity with a laser interferometer. The traces of the direction of deposition are clearly visible on the workpiece. That is why the issue of the anisotropy of the strength properties of this alloy is a concern. It is known that in the process of manufacturing using AM technologies, the material may have anisotropy of properties with respect to the material deposition direction [23]. For the practical use of such materials, it is important to be aware of their anisotropy including that of their mechanical properties. In the present paper, the shock-wave loading experiments were carried out on the alloy

samples along and across the deposition direction as shown in Figure 2. The scheme of the experiments is also shown there.

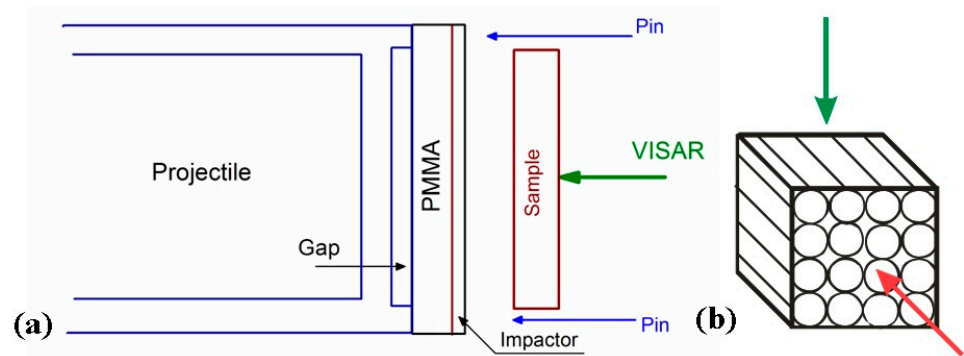


**Figure 2.** The scheme of experiments (a) and the direction of load relative to sample texture (b). Red arrow means load direction along the deposition direction, green means across.

Compression shock waves were generated in the samples under study when the samples collided with 0.1–0.5 mm thick copper impactors accelerated with a 50 mm PP50 pneumatic gun to a velocity of  $340 \pm 10$  m/s, or with 0.4 mm thick aluminum impactors accelerated using special explosive devices [30] to a velocity of  $650 \pm 30$  m/s. The values of the Hugoniot elastic limit and spall strength of the samples under study were determined from the analysis of the velocity profiles of the free surface of the samples. The velocity was continuously recorded during sample loading using a VISAR laser Doppler interferometric velocimeter (Federal Research Center of Problems of Chemical Physics and Medical Chemistry RAS, Chernogolovka, Russia) [31] with a high spatial and temporal resolution. To prevent impactor bending during its acceleration in the gun barrel, the impactor was mounted on a 5 mm thick polymethyl methacrylate substrate with a minimal gap. The substrate was glued to the end of a hollow projectile, a cylinder 50 mm in diameter and 100 mm in length made of D16 grade duralumin. The impactor throwing velocity was measured using electrical contact sensors (pins). The gun barrel and the space around the sample were vacuumized before the experiment. Figure 3 shows visual appearance of the air gun. All the experiments were performed at room temperature.



**Figure 3.** Gas gun for investigating shock-wave phenomena in solids.

### 3. Results and Discussion

Figure 4 shows the velocity profiles of the free surface of samples of the 95% Inconel 625 + 5% NiTi–TiB<sub>2</sub> alloy fabricated in the course of experiments with a light gas gun when loading samples along (a) and across (b) the deposition direction.



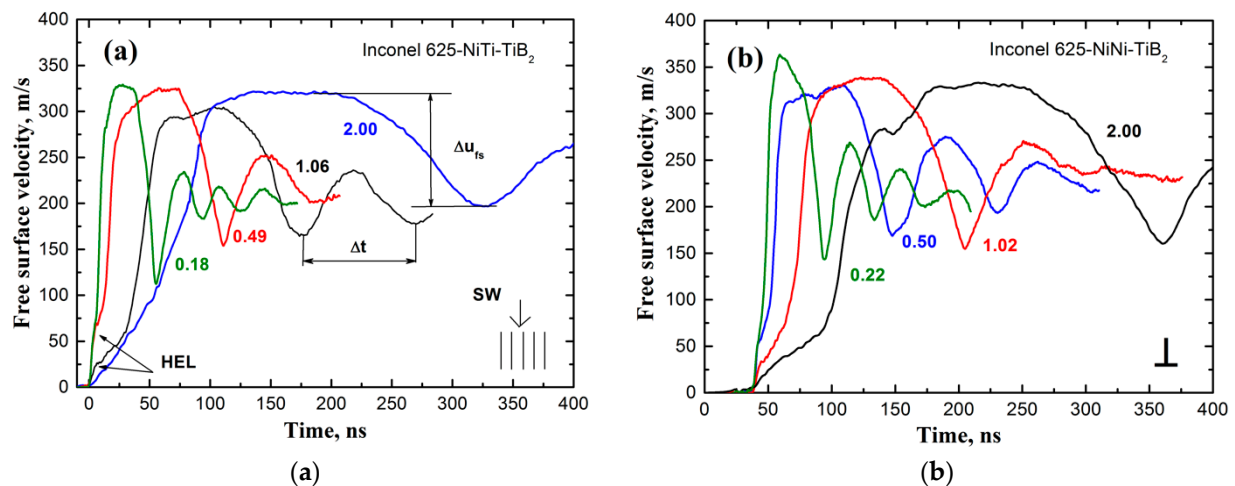


**Figure 4.** Velocity profiles of the free surface of 95% Inconel 625 + 5% NiTi-TiB<sub>2</sub> alloy samples obtained in the experiments with samples loaded along (a) and across (b) the deposition direction.

The wave profiles obtained demonstrate all the features of shock-wave deformation and spall fracture of the samples. The wave front is a two-wave configuration associated with an elastic–plastic transition in the compression wave. The elastic precursor wave propagates ahead of the plastic compression wave with a velocity approximately equaling the longitudinal sound speed. A smooth increase in the parameters between elastic and plastic waves is associated with stress relaxation and strain hardening of the material [32]. In the plastic compression wave, the substance acquires maximum velocity. The stress that corresponded to the Hugoniot elastic limit of the material  $\sigma_{HEL}$  is calculated from the amplitude of the elastic compression wave  $u_{HEL}$  as  $\sigma_{HEL} = \rho_0 C_l u_{HEL} / 2$ , where  $u_{HEL}$  is the maximum surface velocity on the elastic compression wave and  $C_l$  is the longitudinal sound speed.

Maximum shock wave compression pressure was determined as  $P_{max} = \rho_0 U_S u_{max}$  where  $\rho_0$  is the sample density,  $U_S$  is the shock wave velocity and  $u_{max} = W_{max}/2$  is the particle velocity at profile peak. The shock adiabat for calculating the maximum pressure was taken from [27] for Inconel 625 as linear relations  $U_S = 4.497 + 1.61u_p$  (for loading across the deposition direction) and  $U_S = 4.502 + 1.55u_p$  (for loading along the deposition direction) assuming that the adding 5% of the NiTi-TiB<sub>2</sub> dopant will not cause a noticeable error in the calculations. The estimated error associated with the use of adiabats in this form does not exceed 1%, which is somewhat less than the measurement error.

Behind the shock wave, a rarefaction wave emerges on the surface of the sample, reducing its velocity. The first velocity minimum moment in time corresponds to the formation of a spall crack inside the sample when tensile stresses exceeding the strength of the sample are generated inside the sample due to the interaction of the rarefaction waves, one of which is the incident wave and the other one is reflected from the free surface [30]. At the moment of spallation, tensile stresses relax from a value equal to the critical tensile stresses (i.e., the spall strength of the material) to zero, which results in the formation of a weak compression wave (the spall pulse). The value of the decrease in the surface velocity  $\Delta u_{fs}$  (Figure 4) from its maximum to the first minimum before the front of the spall pulse is proportional to the spall strength of the material  $\sigma_{sp}$ . In a linear approximation, the spall strength is defined as  $\sigma_{sp} = 1/2 \rho_0 C_b (\Delta u_{fs} + \delta)$  where  $\delta$  is the correction for the velocity profile distortion caused by the difference in the velocity of the spall pulse front  $C_l$  and the velocity of the plastic part of the incident unloading wave in front of it moving with the bulk speed of the sound ( $C_b$ ) [33].

Spall pulse reverberations in the spall plate cause surface velocity oscillations which are recorded on the profile as decay velocity oscillations. From the time of a single oscillation of the spall pulse  $\Delta t$  (Figure 4) in the spall plate, we can determine its thickness as

$h_{sp} = C_l \Delta t / 2$ . The strain rate of the material before spalling is actually the rate of expansion of the substance in the rarefaction wave and it equals to:

$$\frac{\dot{V}}{V_0} = -\frac{\dot{u}_{f_{sr}}}{2c_b}$$

where  $\dot{u}_{f_{sr}}$  is the decay rate of the free surface velocity in the unloading wave before spalling as determined from the wave profile.

Figures 5 and 6 show the results of processing the wave profiles shown in Figure 4 as a dependency of the Hugoniot elastic limit vs. the distance traveled by the elastic wave and the dependency of the spall strength vs. the strain rate. For the sake of comparison, the Figures 5 and 6 also show values of the strength characteristics of a pure AM Inconel 625 alloy obtained under the similar loading conditions [27]. The experimental conditions and calculated strength characteristics are shown in Table 1.

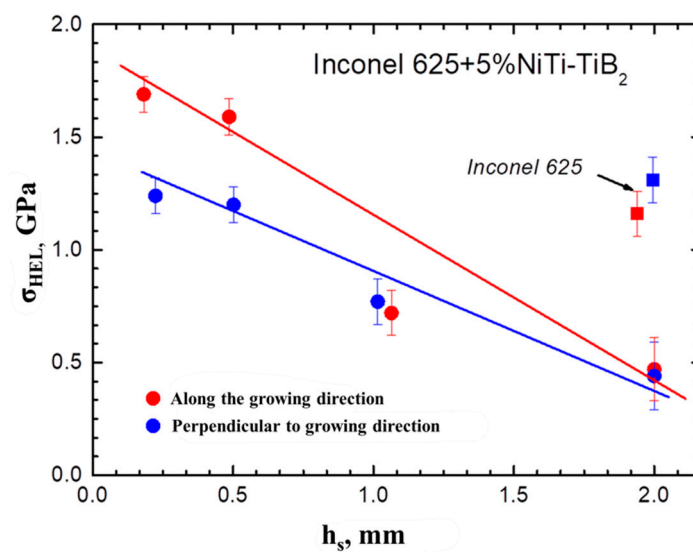


**Figure 5.** Hugoniot elastic limit of the 95% Inconel 625 + 5%NiTi–TiB<sub>2</sub> AM alloy. The data for pure Inconel 625 alloy were taken from [27].

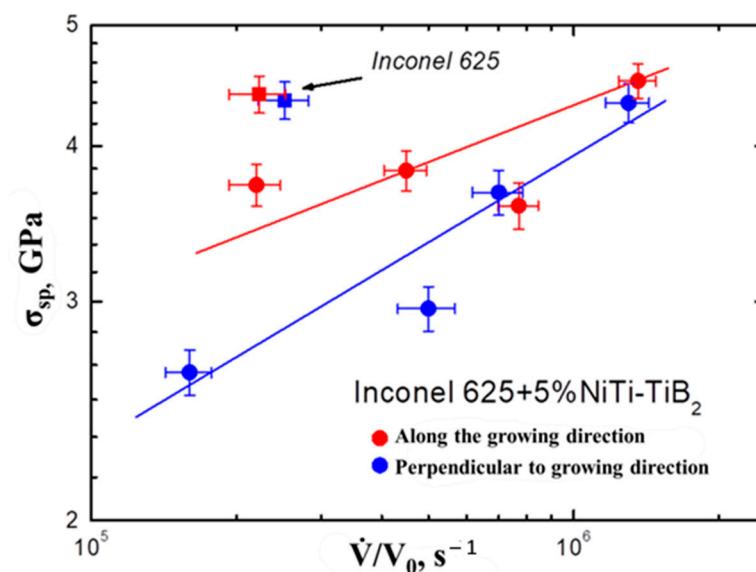


**Figure 6.** Dependency of the spall strength of the 95% Inconel 625 + 5% NiTi–TiB<sub>2</sub> AM alloy on the strain rate before spalling. The data for pure Inconel 625 alloy were taken from [27].

**Table 1.** The conditions and results of the experiments carried out with a PP50 pneumatic gun, and the results of wave profiles processing. Here  $h_{vl}$  is the sample thickness;  $h_{imp}$  is the thickness of the impactor;  $W_{min}$  is the surface velocity before spalling;  $W_{max}$  is the maximum surface velocity;  $P_{max}$  is the maximum shock compression pressure;  $u_{HEL}$  is the elastic precursor wave amplitude;  $\sigma_{HEL}$  is the Hugoniot elastic limit;  $\sigma_{sp}$  is the spall strength;  $\dot{V}/V_0$  is the strain rate in the rarefaction wave,  $\Delta t$  is the time of a single spall pulse oscillation;  $h_{sp}$  is the spall plate thickness.

No	$H_{vl}$ , mm	$H_{imp}$ , mm	$W_{min}$ , m/s	$W_{max}$ , m/s	$P_{max}$ , GPa	$u_{HEL}$ , m/s	$\sigma_{HEL}$ , GPa	$\sigma_{sp}$ , GPa	$\dot{V}/V_0$	$\Delta t$ , ns	$h_{sp}$ , mm
Along the deposition direction											
1	0.19	0.09	112	329	6.45	71	1.69	4.33	$1.3 \times 10^6$	35	0.1
2	0.49	0.19	153	323	6.32	67	1.59	3.67	$7.1 \times 10^5$	91	0.25
3	1.06	0.26	165	305	5.95	26	0.72	2.96	$5.0 \times 10^5$	95	0.27
4 *	2.0	0.44	196	320	6.26	19	0.45	2.63	$1.6 \times 10^5$	212	0.6
Across the deposition direction											
5	0.22	0.09	144	364	7.18	54	1.24	4.51	$1.4 \times 10^6$	40	0.11
6	0.50	0.19	168	331	6.5	52	1.20	3.58	$7.7 \times 10^5$	82	0.23
7	1.02	0.5	154	338	6.64	33	1.77	3.82	$4.5 \times 10^5$	109	0.3
8 *	2.0	0.43	160	334	6.56	19	0.44	3.72	$2.2 \times 10^5$	214	0.6

\* explosive experiments where the velocity of an aluminum impactor was  $650 \pm 30$  m/s [30].

As seen from Figure 5, the Hugoniot elastic limit of the composite alloy decreases noticeably as the elastic wave propagates through the sample. For thin samples, there is a significant difference in its value, which is up to 25%, depending on the loading conditions, while for thicker samples it is practically absent. It means that in the experiments with thin samples, the composite alloy demonstrates noticeable anisotropy of the Hugoniot elastic limit. Overall attenuation of the elastic precursor wave and, accordingly, a decrease in the Hugoniot elastic limit of this alloy in this range of sample thicknesses reaches 75% in experiments with samples loaded along the deposition direction and up to 65% when the samples were loaded across it. It should be noted that under the same loading conditions (sample thickness), the value of the Hugoniot elastic limit measured for pure Inconel 625 alloy [27] exceeds this value measured for the 95% Inconel 625 + 5% NiTi–TiB<sub>2</sub> composite alloy by about 2.5 times.

An analysis of the measurement results of the strength characteristics of the investigated alloy in the conditions of spall fracture (Figure 6) shows that critical fracture stresses (i.e., spall strength) strongly depend on the rate of material strain before fracture. Critical fracture stresses in this range of strain rates increased by up to 40% when the samples were loaded along the deposition direction and they increased by almost 20% when loading across it. It can be seen from the figure that at strain rates below  $5 \times 10^5$  s<sup>−1</sup>, strong anisotropy of spall strength relative to the deposition direction is observed, and the difference in fracture stresses may reach 30%. However, at high strain rates, anisotropy is virtually the same within the measured values scatter for both sample types. The absence of strength anisotropy at high strain rates is explained by the fact that under these conditions, smaller structural defects become the initiators of spall fracture (i.e., tensile stress concentrators) and those are distributed more uniformly within the sample volume and independently of the material texture shaped by the fabrication process. The values of spall strength for pure Inconel 625 alloy [27] obtained for similar loading conditions are also provided here. It can be seen that fracture spall stresses realized in a pure material do not depend on the loading conditions (load direction) and exceed those measured for the composite alloy by 15–40%, depending on the loading direction.

#### 4. Conclusions

Shock wave experiments performed to measure the strength characteristics of a pure high-temperature Inconel 625 alloy and a composite alloy based thereon and consisting of 95% Inconel 625 + 5% NiTi–TiB<sub>2</sub> have produced the following conclusions:

- unlike pure alloy, the 95% Inconel 625 + 5% NiTi–TiB<sub>2</sub> composite alloy demonstrates anisotropy of strength characteristics depending on the direction of material deposition;
- the Hugoniot elastic limit and spall strength of pure Inconel 625 alloy are significantly higher than those measured under the same loading conditions for the composite alloy;
- critical fracture stresses and Hugoniot elastic limit of both alloys do not depend on the intensity of shock compression;
- the spall strength of the composite alloy increases with an increase in the strain rate before fracture, and the Hugoniot elastic limit decreases as the elastic compression wave propagates within the sample, regardless of the loading conditions relative to the sample texture.

**Author Contributions:** Conceptualization, S.R., A.S, V.P. and G.G.; methodology, G.G. and O.K.-K.; investigation, A.M. and A.V.; writing—original draft preparation, A.S., G.G., S.R. and V.P.; writing—review and editing, O.K.-K.; visualization, A.M. All authors have read and agreed to the published version of the manuscript.

**Funding:** The work was supported by the Ministry of Science and Higher Education of the Russian Federation (Agreements with the Joint Institute for High Temperatures RAS No. 075-15-2020-785). Shock wave experiments were carried out on the equipment of the Moscow Regional Explosive Center for Collective Equipment Use of the Russian Academy of Sciences.

**Data Availability Statement:** Not applicable.

**Conflicts of Interest:** The authors declare no conflict of interest.

#### References

1. Fox, G.R.; Liang, H. Wear Mode Comparison of High-Performance Inconel Alloys. *J. Tribol.* **2010**, *132*, 021603. [\[CrossRef\]](#)
2. Wong, K.V.; Hernandez, A. A review of additive manufacturing. *ISRN Mech. Eng.* **2012**, *1*, 1–10. [\[CrossRef\]](#)
3. Raj, B.A.; Jappes, J.T.W.; Khan, M.A.; Dillibabu, V.; Brintha, N.C. Direct metal laser sintered (DMLS) process to develop Inconel 718 alloy for turbine engine components. *Optik* **2020**, *202*, 163735.
4. Schilke, P.W.; Foster, A.D.; Pepe, J.J. *Advanced Gas Turbine Materials and Coatings*; General Electric Company: New York, NY, USA, 1991.
5. Sharma, P.; Chakradhar, D.; Narendranath, S. Evaluation of WEDM performance characteristics of Inconel 706 for turbine disk application. *Mater. Des.* **2015**, *88*, 558–566. [\[CrossRef\]](#)
6. Farid, A.A.; Sharif, S.; Namazi, H. Effect of machining parameters and cutting edge geometry on surface integrity when drilling and hole making in Inconel 718. *SAE Int. J. Mater. Manuf.* **2009**, *2*, 564–569. [\[CrossRef\]](#)
7. Rao, H.; Oleksak, R.P.; Favara, K.; Harooni, A.; Dutta, B.; Maurice, D. Behavior of yttria-stabilized zirconia (YSZ) during laser direct energy deposition of an Inconel 625-YSZ cermet. *Addit. Manuf.* **2020**, *31*, 100932. [\[CrossRef\]](#)
8. Zhukov, I.A.; Kozulin, A.A.; Khrustalyov, A.P.; Matveev, A.E.; Platov, V.V.; Vorozhtsov, A.B.; Zhukova, T.V.; Promakhov, V.V. The Impact of Particle Reinforcement with Al<sub>2</sub>O<sub>3</sub>, TiB<sub>2</sub>, and TiC and Severe Plastic Deformation Treatment on the Combination of Strength and Electrical Conductivity of Pure Aluminum. *Metals* **2019**, *9*, 65. [\[CrossRef\]](#)
9. Matveev, A.; Zhukov, I.; Ziatdinov, M.; Zhukov, A. Planetary Milling and Self-Propagating High-Temperature Synthesis of Al–TiB<sub>2</sub> Composites. *Materials* **2020**, *13*, 1050. [\[CrossRef\]](#)
10. Hashim, J.; Looney, L.; Hashmi, M.S. Metal matrix composites: Production by the stir casting method. *J. Mater. Process. Technol.* **1999**, *92*, 1–7. [\[CrossRef\]](#)
11. Tjong, S.C. Novel nanoparticle-reinforced metal matrix composites with enhanced mechanical properties. *Adv. Eng. Mater.* **2007**, *9*, 639–652. [\[CrossRef\]](#)
12. Vorozhtsov, S.A.; Eskin, D.G.; Tamayo, J.; Vorozhtsov, A.B.; Promakhov, V.V.; Averin, A.A.; Khrustalyov, A.P. The application of external fields to the manufacturing of novel dense composite master alloys and aluminum-based nanocomposites. *Metall. Mater. Trans. A* **2015**, *46*, 2870–2875. [\[CrossRef\]](#)
13. Rawal, S.P. Metal-matrix composites for space applications. *JOM* **2001**, *53*, 14–17. [\[CrossRef\]](#)
14. Wilson, J.M.; Shin, Y.C. Microstructure and wear properties of laser-deposited functionally graded Inconel 690 reinforced with TiC. *Surf. Coat. Technol.* **2012**, *207*, 517–522. [\[CrossRef\]](#)



15. Liu, Z.; Cabrero, J.; Niang, S.; Al-Taha, Z.Y. Improving corrosion and wear performance of HVOF-sprayed Inconel 625 and WC-Inconel 625 coatings by high power diode laser treatments. *Surf. Coat. Technol.* **2007**, *201*, 7149–7158. [\[CrossRef\]](#)
16. Nurminen, J.; Näkki, J.; Vuoristo, P. Microstructure and properties of hard and wear resistant MMC coatings deposited by laser cladding. *Int. J. Refract. Met. Hard Mater.* **2009**, *27*, 472–478. [\[CrossRef\]](#)
17. Promakhov, V.; Matveev, A.; Klimova-Korsmik, O.; Schulz, N.; Bakhmat, V.; Babaev, A.; Vorozhtsov, A. Structure and Properties of Metal-Matrix Composites Based on an Inconel 625–TiB<sub>2</sub> System Fabricated by Additive Manufacturing. *Metals* **2022**, *12*, 525. [\[CrossRef\]](#)
18. Matveev, A.; Promakhov, V.; Schulz, N.; Bakhmat, V.; Babaev, A.; Semenov, A.; Vorozhtsov, A. Effect of the Mass Fraction of NiTi–TiB<sub>2</sub> SHS-Particles on the Phase Composition, Structure, and Mechanical Properties of Inconel 625–NiTi–TiB<sub>2</sub> Composites Produced by Direct Laser Deposition. *Materials* **2022**, *15*, 6861. [\[CrossRef\]](#) [\[PubMed\]](#)
19. Arlyapov, A.; Volkov, S.; Promakhov, V.; Matveev, A.; Babaev, A.; Vorozhtsov, A.; Zhukov, A. Study of the Machinability of an Inconel 625 Composite with Added NiTi–TiB<sub>2</sub> Fabricated by Direct Laser Deposition. *Metals* **2022**, *12*, 1956. [\[CrossRef\]](#)
20. Wise, J.L.; Adams, D.P.; Nishida, E.E.; Song, B.; Maguire, M.C.; Carroll, J.; Reedlunn, B.; Bishop, J.E.; Palmer, T.A. Comparative shock response of additively manufactured versus conventionally wrought 304L stainless steel. *AIP Conf. Proc.* **2017**, *1793*, 100015.
21. Klimova-Korsmik, O.; Turichin, G.; Mendagaliyev, R.; Razorenov, S.; Garkushin, G.; Savinykh, A.; Korsmik, R. High-Strain Deformation and Spallation Strength of 09CrNi2MoCu Steel Obtained by Direct Laser Deposition. *Metals* **2021**, *11*, 1305. [\[CrossRef\]](#)
22. Brown, A.D.; Ameri, A.H.; Gregg, A.; Austin, D.C.; Escobedo, J.P.; Hazell, P.J.; East, D.; Quadir, M.Z. Dynamic mechanical response of additive manufactured Ti-6Al-4V. *AIP Conf. Proc.* **2018**, *1979*, 070008.
23. Jones, D.R.; Fensin, S.J.; Dippo, O.; Beal, R.A.; Livescu, V.; Martinez, D.T.; Trujillo, C.P.; Florando, J.N.; Kumar, M.; Gray III, G.T. Spall fracture in additive manufactured Ti-6Al-4V. *J. Appl. Phys.* **2016**, *120*, 135902. [\[CrossRef\]](#)
24. Razorenov, S.V.; Garkushin, G.V.; Savinykh, A.S.; Klimova-Korsmik, O.G.; Shalnova, S.A.; Gushchina, M.O. Dynamic Strength of VT6 Titanium Alloy Manufactured by Laser Metal Deposition. *Phys. Mesomech.* **2022**, *25*, 26–32. [\[CrossRef\]](#)
25. Zaretsky, E.; Stern, A.; Frage, N. Dynamic response of AlSi10Mg alloy fabricated by selective laser melting. *Mater. Sci. Eng. A* **2017**, *688*, 364–370. [\[CrossRef\]](#)
26. Gray, G.T., III; Knapp, C.M.; Jones, D.R.; Livescu, V.; Fensin, S.; Morrow, B.M.; Trujillo, C.P.; Martinez, D.T.; Valdez, J.A. Structure/property characterization of spallation in wrought and additively manufactured tantalum. *AIP Conf. Proc.* **2018**, *1979*, 060002.
27. Promakhov, V.; Schulz, N.; Vorozhtsov, A.; Savinykh, A.; Garkushin, G.; Razorenov, S.; Klimova-Korsmik, O. The Strength of Inconel 625, Manufactured by the Method of Direct Laser Deposition under Sub-Microsecond Load Duration. *Metals* **2021**, *11*, 1796. [\[CrossRef\]](#)
28. Savinykh, A.S.; Garkushin, G.V.; Razorenov, S.V.; Atroshenko, S.A.; Klimova-Korsmik, O.G.; Kislov, N.G. Strength Properties of the Heat-Resistant Inconel 718 Superalloy Additively Manufactured by Direct Laser Deposition Method under Shock Compression. *Metals* **2022**, *12*, 967. [\[CrossRef\]](#)
29. Razorenov, S.V.; Savinykh, A.S.; Garkushin, G.V.; Atroshenko, S.A. Effect of Heat Treatment and Test Temperature on the Strength Properties of Cast Heat-Resistant Nickel Base Inconel 718 Superalloy under Shock-Wave Loading. *Metals* **2022**, *12*, 1098. [\[CrossRef\]](#)
30. Antoun, T.; Curran, D.R.; Razorenov, S.V.; Seaman, L.; Kanel, G.I.; Utkin, A.V. *Spall fracture*; Springer: New York, USA, 2003.
31. Barker, L.M.; Hollenbach, R.E. Laser interferometer for measuring high velocities of any reflecting surface. *J. Appl. Phys.* **1972**, *43*, 4669–4675. [\[CrossRef\]](#)
32. Kanel, G.I. *Shock Waves in Solid state Physics*; CRC Press: Boca Raton, FL, USA; Taylor and Francis Group: London, UK; New York, NY, USA.
33. Kanel, G.I. Spall fracture: Methodological aspects, mechanisms and governing factors. *Int. J. Fract.* **2010**, *163*, 173–191. [\[CrossRef\]](#)

**Disclaimer/Publisher’s Note:** The statements, opinions and data contained in all publications are solely those of the individual author(s) and contributor(s) and not of MDPI and/or the editor(s). MDPI and/or the editor(s) disclaim responsibility for any injury to people or property resulting from any ideas, methods, instructions or products referred to in the content.